

1 **Quantifying inclination shallowing and representing
2 flattening uncertainty in sedimentary paleomagnetic
3 poles**

4 **James Pierce^{1,2}, Yiming Zhang¹, Eben B. Hodgin¹, Nicholas L.
5 Swanson-Hysell¹**

6 ¹Department of Earth and Planetary Science, University of California, Berkeley, CA, USA

7 ²Department of Earth and Planetary Sciences, Yale University, New Haven, CT, USA

8 **Key Points:**

- 9 • Inclination shallowing is empirically quantified in 1.1 Ga clastic sedimentary rocks
10 bracketed by volcanics
- 11 • Detrital hematite remanence is flattened by a factor of $0.61_{0.55}^{0.67}$ relative to unflat-
12 tened pigmentary hematite
- 13 • Flattening factor uncertainty is present in all methods and should be incorporated
14 into the uncertainty of sedimentary paleomagnetic poles

Corresponding author: James Pierce (james.pierce@yale.edu); Nicholas Swanson-Hysell
(swanson-hysell@berkeley.edu),

15 **Abstract**

Inclination is the angle of a magnetization vector from horizontal. Clastic sedimentary rocks often experience inclination shallowing whereby syn- to post-depositional processes result in flattened detrital remanent magnetizations relative to local geomagnetic field inclinations. The deviation of recorded inclinations from true values presents challenges for reconstructing paleolatitudes. A widespread approach for estimating flattening factors (f) compares the shape of an assemblage of magnetization vectors to that derived from a paleosecular variation model (the elongation/inclination [E/I] method). Few studies exist that compare the results of this statistical approach with empirically determined flattening factors and none in the Proterozoic Eon. In this study, we evaluate inclination shallowing within 1.1 billion-year-old, hematite-bearing red beds of the Cut Face Creek Sandstone that is bounded by lava flows of known inclination. Taking this inclination from the volcanics as the expected direction, we found that detrital hematite remanence is flattened with $f = 0.65^{0.75}_{0.56}$ whereas the pigmentary hematite magnetization shares a common mean with the volcanics. Using the pigmentary hematite direction as the expected inclination results in $f = 0.61^{0.67}_{0.55}$. These flattening factors are consistent with those estimated through the E/I method ($f = 0.64^{0.85}_{0.51}$) supporting its application in deep time. However, all methods have significant uncertainty associated with determining the flattening factor. This uncertainty can be incorporated into paleomagnetic poles with the resulting ellipse approximated with a Kent distribution. Rather than seeking to find “the flattening factor,” or assuming a single value, the inherent uncertainty in flattening factors should be recognized and incorporated into paleomagnetic syntheses.

38 **Plain Language Summary**

The magnetization of ancient sedimentary rocks provides great insight into Earth’s past. Earth scientists use these rocks to understand how Earth’s magnetic field has flipped through time and to reconstruct how continents have moved. Hematite is a common mineral which gives many sandstones a red color — leading geologists to refer to them as “red beds.” While hematite is a reliable magnet through time, the magnetic directions recorded by hematite grains can be shallower than the geomagnetic field (i.e. they are flattened). Magnetization steepness is how Earth scientists determine the latitude where rocks were deposited as the magnetic field gets steeper towards the pole. We need ways

47 to correct for magnetization shallowing in sedimentary rocks. In this study, we compared
 48 the steepness of magnetic directions held by hematite to that of lava flows that formed
 49 in the same time interval. Magnetic directions from lava flows are not flattened so this
 50 comparison allows us to determine the shallowing amount. We compare it to a statisti-
 51 cal method and see that the results are indistinguishable within the appreciable un-
 52 certainty of the methods. Earth scientists should include the uncertainty associated with
 53 inclination shallowing when they report ancient pole positions determined from such flat-
 54 tened magnetic directions.

55 1 Introduction

Hematite-bearing sedimentary rocks at Earth's surface are widespread and serve as an important paleomagnetic recorder. The geocentric axial dipole (GAD) hypothesis posits that the long-term average of Earth's magnetic field is dipolar and that the time-averaged geomagnetic pole overlaps with the geographic pole. Using this hypothesis, the inclination (I) of a rock's magnetization can be translated into an interpreted paleolatitude (ϕ) of the location where the rock formed using the dipole formula:

$$\tan(I) = 2 \tan(\phi)$$

56 Unfortunately, the accuracy of paleomagnetic directions recorded by the detrital rema-
 57 nent magnetization (DRM) of sedimentary rocks has long been recognized as problem-
 58 atic due to the issue of inclination shallowing (King, 1955; van Andel & Hespers, 1966;
 59 Tauxe & Kent, 1984; Kodama, 2012). The rotation of ferromagnetic grains during de-
 60 position and compaction can result in the acquisition of a detrital remanent magneti-
 61 zation that is biased shallow relative to the local geomagnetic field in which it was ac-
 62 quired (Tauxe, 2005). If uncorrected, shallower inclinations obtained from sedimentary
 63 rocks can potentially result in erroneously low estimates of paleolatitudes, biasing the
 64 interpreted past positions of continents and hindering plate reconstructions. Despite this
 65 challenge, the abundance and long-term magnetic and geochemical stability of hematite
 66 makes hematite-bearing sedimentary rocks a very important archive of Earth history.

67 In addition to detrital hematite grains that can carry a DRM, hematite-bearing
 68 sedimentary rocks often have a distinct population of pigmentary hematite that give "red
 69 beds" their characteristic red color. This finer-grained pigmentary hematite precipitates
 70 following deposition and carries a chemical remanent magnetization (CRM) acquired dur-

71 ing crystal growth (Tauxe et al., 1980; Jiang et al., 2015; Swanson-Hysell et al., 2019).
 72 This pigmentary hematite can form from metastable Fe(III) oxide precursors such as fer-
 73 rihydrite (Gutiérrez et al., 2016; Jiang et al., 2018, 2022). Such pigmentary hematite records
 74 a magnetization when it grows to be the size of a stable single domain particle (~ 30 nm;
 75 Özdemir and Dunlop (2014)). Although the CRMs acquired by pigmentary hematite are
 76 not expected to be shallowed, the time lag between sediment deposition and secondary
 77 pigmentary hematite formation can be variable which complicates interpretations. For-
 78 tunately, magnetization held by primary detrital hematite can be isolated from that held
 79 by finer-grained secondary pigmentary hematite through high resolution thermal demag-
 80 netization as hematite grains less than ~ 400 nm in diameter will unblock at lower tem-
 81 peratures than coarser detrital grains (Tauxe et al., 1980; Swanson-Hysell et al., 2019).
 82 After thermal demagnetization of pigmentary hematite, the DRM held by coarser hematite
 83 grains will become apparent near hematite's Néel Temperature ($\sim 682^\circ\text{C}$; Butler (1992);
 84 Lu and Meng (2010)).

To elucidate factors that contribute to inclination shallowing of detrital magnetization in sedimentary rocks, King (1955) conducted laboratory redeposition experiments and quantified the shallowing effect with the flattening function:

$$\tan(I_o) = f \tan(I_f)$$

85 where I_o represents the observed inclination of the specimen magnetization and I_f rep-
 86 resents the inclination of the field in which the magnetization was acquired (Fig. 1). The
 87 flattening factor f ranges from 1 for no flattening to 0 for completely flattened inclina-
 88 tions (Fig. 1). Further laboratory redeposition experiments have found that major con-
 89 tributing processes to inclination shallowing include the initial settling and deposition
 90 of particles as well as compaction during burial (Anson & Kodama, 1987; Tauxe & Kent,
 91 1984; Sun & Kodama, 1992; Tan et al., 2002). The degree of flattening can also be in-
 92 fluenced by sedimentary lithology with finer grained sediments exhibiting more inclina-
 93 tion shallowing in laboratory experiments (Tan et al., 2002).

94 Correcting the effects of inclination shallowing is crucial for estimating the incli-
 95 nation of the geomagnetic field at the time of deposition. Two main classes of correc-
 96 tion methods have been developed and applied in order to determine and correct for in-
 97 clination shallowing. The first class of methods involves investigating the magnetic fab-
 98 rics of the sedimentary rocks of interest. Such an approach was pioneered by Jackson

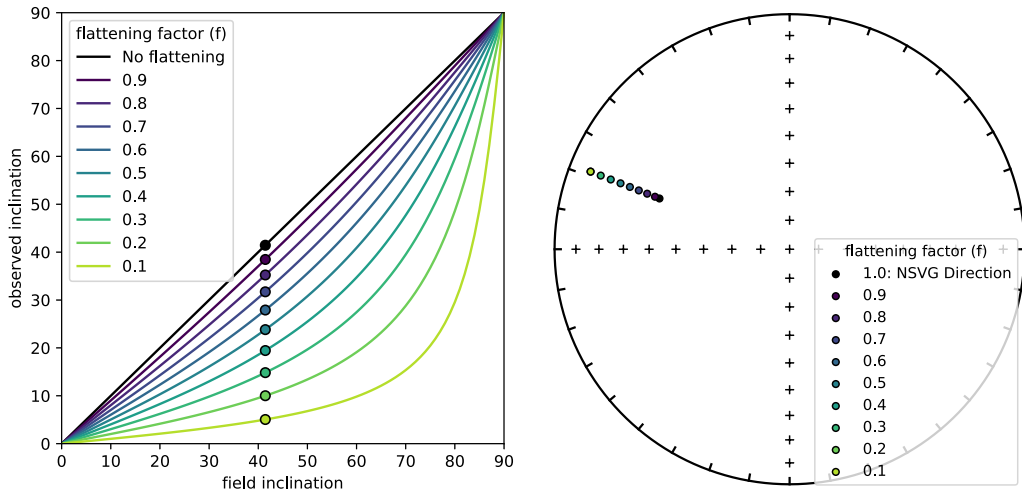


Figure 1: Left panel: the relationship between the inclination of the local magnetic field compared to the observed inclination of sedimentary rocks is shown for different flattening factors (f). A value of 1.0 corresponds to no flattening while a value of 0.0 means the magnetizations are completely flattened. The dots show the inclination expected for the Cut Face Creek Sandstone that would result from variable flattening of the mean inclination of lavas from the upper northeast sequence of the North Shore Volcanic Group (NSVG; Tauxe and Kodama (2009); Swanson-Hysell et al. (2019)). Right panel: an equal area plot with the mean paleomagnetic direction of the upper northeast sequence North Shore Volcanic Group lavas (declination of 290.7°; inclination of 41.4°) and the directions that would result from applying different flattening factors.

et al. (1991), where anisotropy of anhysteretic magnetization (AARM) was used to estimate and correct shallowed inclinations. Subsequent work has highlighted the importance of determining the relationship between shallowing and magnetic anisotropy associated with a given sedimentary rock in the application of the method (Kodama, 2012). A particular difficulty in applying this method to correct detrital remanent magnetizations in hematite-bearing sedimentary rocks is that both pigmentary hematite and detrital hematite contribute to the overall magnetic fabric with the anisotropy associated with the detrital population needing to be isolated for an inclination shallowing correction. Recognizing this challenge, Bilardello (2015) developed a more involved multispecimen approach using step-wise thermal demagnetization of applied isothermal remanent magnetizations (IRM) in order to isolate the anisotropy of DRM. Overall, such anisotropy approaches are labor-intensive and have only been applied to quantify inclination shallowing in a modest number of studies.

The other principal method for correcting inclination shallowing is the statistical elongation/inclination (E/I) approach (Tauxe & Kent, 2004). This method utilizes the

fact that inclination shallowing will skew the shape of the population of recorded magnetization vectors away from a distribution expected from secular variation of Earth's magnetic field. The E/I method uses the TK03 model for paleosecular variation which is based on a compilation of paleomagnetic directions from lava flows of the last 5 million years (McElhinny & McFadden, 1997) to predict the original distribution and shape of paleomagnetic directions based on a Giant Gaussian Process approach. In this model, the distribution of paleomagnetic directions at a given latitude that sufficiently samples paleosecular variation has a predictable elongated shape that deviates from circular symmetry as a function of inclination. The shape of the distribution of vectors is quantified by the elongation parameter (E) that can be determined by calculating the eigenvalue ratio τ_2/τ_3 of the orientation matrix for a population of vectors. One can estimate the amount of inclination shallowing in a sedimentary rock by progressively unflattening the shallowed magnetization vectors until their distribution best matches the predicted shape. This approach assumes that the TK03.GAD model accurately characterizes the paleosecular variation during acquisition of magnetization in the sedimentary formation of interest. The uncertainty on the flattening factor that leads to a correspondence between the elongation of the magnetization vectors with the E/I of the TK03.GAD model can be estimated through bootstrap resampling (Tauxe & Kent, 2004). As a statistical method, the E/I has the benefit that the analyses are done on specimen DRM magnetization directions and it does not require additional labor-intensive anisotropy measurements which includes the necessary determination of individual particle anisotropy. However, this method requires a large number of distinct DRM directions (>100) as many more vectors are needed to accurately determine the shape of a distribution than the mean of a distribution (Tauxe et al., 2008). Where <100 directions are used to determine a flattening factor through the E/I method, the associated uncertainty associated with the flattening factor estimate can exceed that of anisotropy-based methods (Bilardello et al., 2011). The large number of directions needed to reliably apply the method led Vaes et al. (2021) to propose a classification scheme wherein >100 directions are needed for a corrected sedimentary pole to be deemed reliable (as well as paleosecular variation being assessed using the criteria of Deenen et al. (2011)).

Due to the challenges of applying these inclination correction methods, particularly to previously published data, another simplified approach that has been taken in the literature is to apply summary statistics from compiled f factors and apply them to the

mean direction calculated from a sedimentary rock (Bilardello & Kodama, 2008, 2009). For many published data sets from sedimentary rocks where the specimen level data are not available and compilations are reliant on study level means, such an approach is the only one that can be applied without redoing the study. This approach was applied by Torsvik et al. (2012) in their compilation of Phanerozoic paleomagnetic poles where a flattening factor of 0.6 was used to correct sedimentary poles. Domeier et al. (2012) also adopted a flattening factor of 0.6 acknowledging that to do so is an oversimplification, but a value that is consistent with compiled f factor estimates (such as those of Bilardello and Kodama (2010c)). This approach has been criticized as disregarding the variability of f factors that can result from differences in lithology and magnetic carriers (Bilardello, 2016; Vaes et al., 2021). There have been other data analysis approaches to seek to constrain f factors such as through comparing intersecting great circles from multiple paleomagnetic poles (Bazhenov & Shatsillo, 2010; Gallo et al., 2017). For any method, there is a challenge of applying a single f factor to a sedimentary formation given variability associated with grain size and other conditions.

In this study, we use the ca. 1093 Ma Cut Face Creek Sandstone to empirically constrain the magnitude of inclination shallowing. The Cut Face Creek Sandstone is a ~95 meter-thick interval of interflow red siltstone and sandstone deposited in a fluvial overbank depositional environment between lava flows of the upper northeast sequence of the North Shore Volcanic Group (Fig. 2). Since the sandstone is bracketed by lava flows with known age and existing paleomagnetic data, its age and expected paleomagnetic direction is well constrained (Tauxe & Kodama, 2009; Swanson-Hysell et al., 2019). We compare the detrital remanence directions of the Cut Face Creek specimens to the expected directions from the volcanics to determine the amount of inclination shallowing that took place within the sedimentary unit. Next, we apply the elongation/inclination method to the isolated DRM directions to obtain statistical estimates for the amount of shallowing that can be compared to the empirically determined value. Finally, we present recommendations for the incorporation of uncertainties in flattening factor estimates into sedimentary paleomagnetic poles and paleolatitude estimates as such uncertainties are present regardless of the method through which they are determined.

177 2 Geologic Setting and stratigraphy of the Cut Face Creek Sandstone

178 The Mesoproterozoic Midcontinent Rift is a protracted intracontinental rift punc-
 179 tuated by rapid and voluminous magmatism throughout its history (Fig. 2A; Green (1983);
 180 Swanson-Hysell et al. (2021)). A ~8 km thick succession of lava flows that erupted dur-
 181 ing Midcontinent Rift development is exposed in northeastern Minnesota forming the
 182 northeast sequence of the North Shore Volcanic Group (Fig. 2B; Green et al. (2011)).
 183 Our study is focused on the ~95-meter-thick Cut Face Creek Sandstone which is an in-
 184 terflow fluvial siliciclastic unit that was deposited during a hiatus in lava flow eruptions
 185 (Jirsa, 1984). It is bracketed by the underlying Good Harbor Bay andesites and the over-
 186 lying Terrace Point Basalt (Figs. 2C and 3). These units are all part of the normal-polarity
 187 upper northeast sequence of the North Shore Volcanic Group (Figs. 2; Green et al. (2011)).
 188 This interval of normal geomagnetic polarity from ca. 1098 to <1083 Ma has been termed
 189 the Keweenawan N superchron (Driscoll & Evans, 2016) and makes it such that no re-
 190 versals are expected during deposition of the Cut Face Creek Sandstone. The Grand Marais
 191 Rhyolite with a high-precision weighted mean $^{206}\text{Pb}/^{238}\text{U}$ zircon date of 1093.52 ± 0.43
 192 Ma (Swanson-Hysell et al., 2019) is ~250 m stratigraphically below the Good Harbor
 193 Bay andesites (Green et al., 2011). Its age serves as a maximum age constraint for the
 194 deposition of Cut Face Creek Sandstone and is likely close to the absolute age. The min-
 195 imum depositional age of the sandstone is constrained by the 1091.7 ± 0.2 Ma Beaver
 196 River diabase of the Beaver Bay Complex, which crosscuts the North Shore Volcanic Group
 197 (Zhang et al., 2021). Paleomagnetic data from twenty-eight lava flows of the upper North-
 198 east sequence of the North Shore Volcanic Group (blue diamonds in Fig. 2; Books (1972);
 199 Tauxe and Kodama (2009)) result in a paleomagnetic pole at 181.7°E , 31.1°N ($A_{95}=4.2^\circ$;
 200 Swanson-Hysell et al. (2019)). This pole from the volcanics can be used to calculate an
 201 expected paleomagnetic direction for the Cut Face Creek Sandstone with a declination
 202 of 290.7° and an inclination of 41.4° (Fig. 1).

203 The Cut Face Creek Sandstone is well-exposed in a prominent roadcut along Min-
 204 nesota State Highway 61 with a striking deep red color (47.7280°N , 90.4428°W ; Figs. 2
 205 and 3). Throughout the section, the strata are consistently tilted to the southeast with
 206 an average dip direction of 166.5° and dip of 10.0° (based on 44 measurements). Our strati-
 207 graphic section through the ~95-meter-thick Cut Face Creek Sandstone was measured
 208 at a decimeter scale upward from its base where it overlies the uppermost lava flow of
 209 the Good Harbor Bay andesites (Fig. 3).

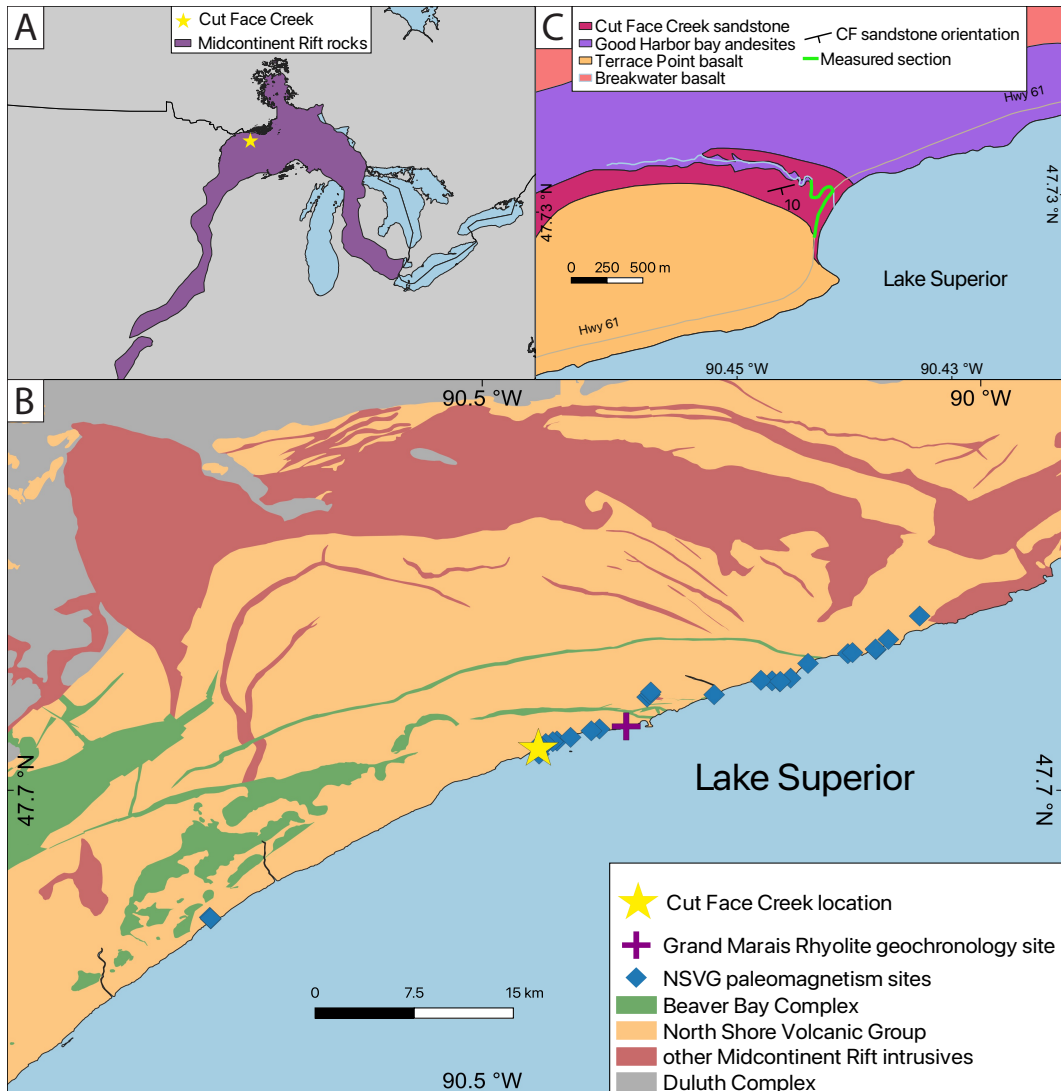


Figure 2: A) Overview map showing the location of the Cut Face Creek Sandstone (yellow star; 47.7280°N, 90.4428°W) within the extent of the Midcontinent Rift. B) Geologic map along the North Shore of Lake Superior showing the location of the Cut Face Creek Sandstone (yellow star) within the upper northeast sequence of the North Shore Volcanic Group (NSVG; geologic data from Miller et al. (2001)). CA-ID-TIMS $^{206}\text{Pb}/^{238}\text{U}$ dates constrain the Cut Face Creek Sandstone to be younger than the 1093.52 ± 0.43 Ma Grand Marais Rhyolite (purple cross; Swanson-Hysell et al. (2019)) and older than the 1091.7 ± 0.2 Ma cross-cutting Beaver River diabase of the Beaver Bay Complex (green unit, Zhang et al. (2021)). C) The Cut Face Creek Sandstone overlies the Good Harbor Bay andesite (purple) while the Terrace Point basalt (tan orange) erupted atop the sandstone. The green line indicates the location of the measured stratigraphic section shown in Fig. 3.

The Good Harbor Bay andesites are fine-grained, greenish-grey, volcanic rocks that become increasingly vesicular toward flow tops. In the measured stratigraphic section, the uppermost lava is overlain by a 0.9-meter-thick silt-sized matrix-supported basalt pebble conglomerate with sand lenses and mud cracks (Fig. 3). This conglomerate is fol-

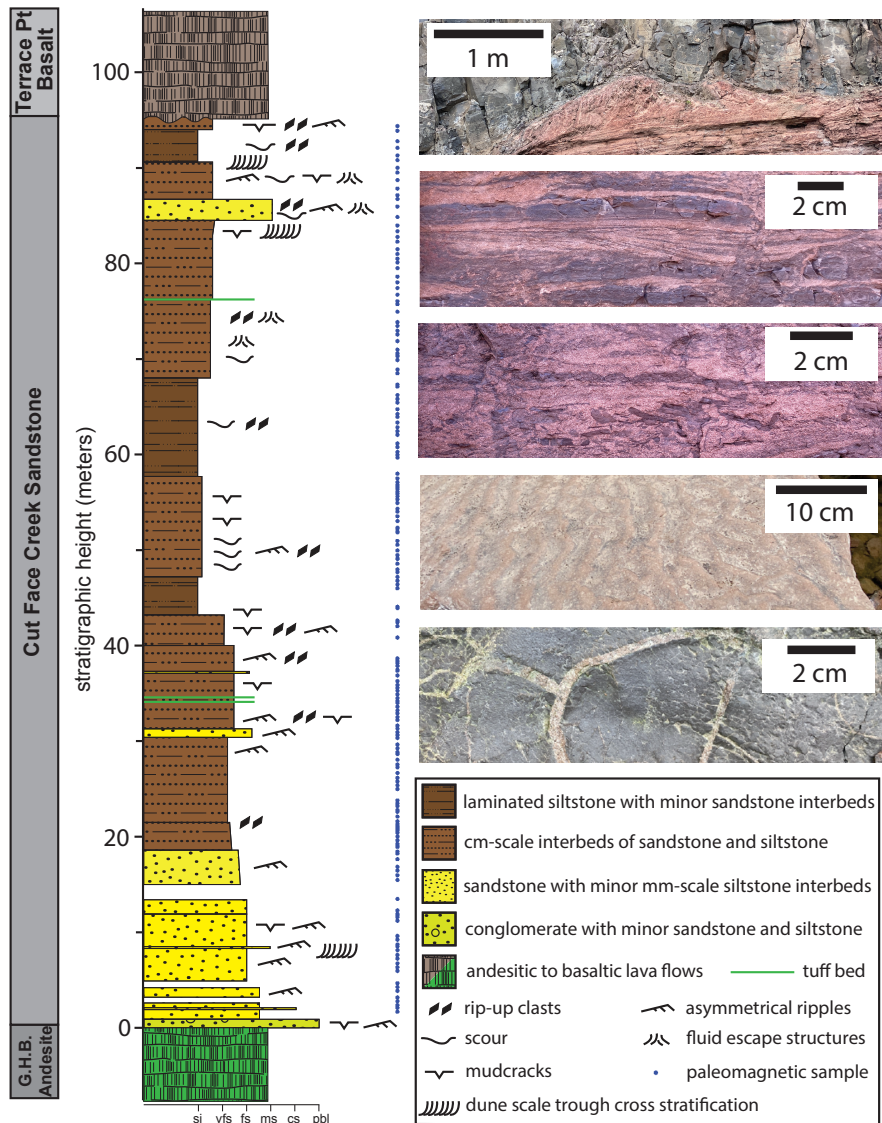


Figure 3: Stratigraphic column of the 95-meter-thick Cut Face Creek Sandstone as exposed along Cut Face Creek and Hwy 61 (Fig. 2). The Cut Face Creek Sandstone was deposited during a hiatus in eruption of the North Shore Volcanic Group lavas such that it is bracketed by the Good Harbor Bay andesites (G.H.B.; green) and the Terrace Creek Basalt (grey). Photos from bottom to top: top view of a mud-cracked siltstone layer within the basal conglomerate; oblique top view of current ripples in sandstone; side view of sandstone (light red) with tabular rip-up clasts of siltstone (dark red); side view of finely interbedded siltstone (dark red) and sandstone (light red) with asymmetric scour and ripple cross-stratification with fluid escape structures; upper contact with Terrace Point Basalt whose advance led to soft sediment deformation in the underlying Cut Face Creek Sandstone.

214 followed by ~17.5 m of medium to fine-grained lithic arkose that generally fines upwards.
 215 The medium-grained sandstone is associated with occasional decimeter-scale dune-scale
 216 trough cross-bedding characteristic of channel bars. Finer-grained sandstone beds that
 217 contain regular mm-scale siltstone laminae, mudcracks, and current ripples with vari-

able flow directions, are characteristic of crevasse splay deposits which occur when a stream overflows its channel leading to overbank deposition (e.g. van Toorenenburg et al., 2018). The next ~11.8 m of strata continue to fine upwards and are dominated by very fine to fine-grained sandstone containing interbeds of cm-scale siltstone. This interval, which contains siltstone rip-up clasts and current ripples with variable flow directions (Fig. 3), is characteristic of continued aggradation of crevasse splay deposits situated farther from the fluvial channel than the underlying interval. At 30.4 m, the stratigraphic trend is disrupted by a similar fining-upwards interval with a basal 1.1 m layer of medium-grained sandstone containing current ripples grading up into ~11.7 m of fine to very fine-grained sandstone with regular interbeds of cm-scale siltstone, which by the top of the interval are subequal in thickness. This interval contains cream-colored ash beds, mudcracks, current ripples, and siltstone rip-up clasts consistent with an increasingly distal overbank environment. The overlying ~41.3 m of strata is dominated by laminated siltstone, and contains regular occurrences of mudcracks and siltstone rip-up clasts—consistent with floodplain sedimentation. Within this interval, fine-grained sandstone is deposited in cm-scale sheets characteristic of distal crevasse splay flooding events and in decimeter-scale asymmetric scours characteristic of meandering channels within a floodplain (Cant & Walker, 1976), with the latter occasionally infilled by dune-scale trough cross-bedding. The upper ~15 m of the siltstone-dominated interval, coarsens upwards, and contains strata that can be disrupted by dewatering structures and infilled cracks that may be attributed to a combination of desiccation, shrinkage, and compaction (Fig. 3). The upper ~10.6 m of the stratigraphic section coarsens upwards from ~30% siltstone to well-lithified fine-to medium-grained sandstone, which was likely deposited in a crevasse splay environment in proximity to a fluvial channel. Flame structures associated with dewatering are common throughout the top part of the section (Fig. 3) with some ripple-scale cross-bedding. The uppermost 5 m include light tan colored horizons (Fig. 3) associated with fluid flow and reduction of the pigmentary hematite. The top 1.1 m beneath the Terrace Point basalt consists of baked siltstone with mudcracks and slaty cleavage. Eruption of the overlying lava flow of the Terrace Point basalt folded and deformed the uppermost sediment layers as it advanced and “bulldozed” the unconsolidated sediment (Fig 3).

Overall, these observations and interpretations are consistent with those of Jirsa (1984) and Mitchell and Sheldon (2009) who invoke a fluvial depositional environment dominated by overbank deposition. Flow in this fluvial system was dominantly to the

251 SSW with the composition of sandstone consistent with a provenance largely derived from
252 the local North Shore Volcanic Group (Jirsa, 1984).

253 **3 Methods**

254 Paleomagnetic cores from the Cut Face Creek Sandstone were sampled through the
255 strata with an interval of ~50 cm (Fig. 3). In order to maximize sampling of paleosec-
256 ular variation, we optimized for vertical stratigraphic coverage and collected one sam-
257 ple at each horizon. As such, each sample constitutes a paleomagnetic site considering
258 that a paleomagnetic site (which ideally captures a single snapshot of the local geomag-
259 netic field) is a particular bed in a sedimentary sequence. Dark red fine-grained siltstone
260 layers were preferentially sampled as they have lower permeability and are less suscep-
261 tible to diagenetic alteration through fluid flow than coarser grained sandstone. Care was
262 taken to avoid samples containing reoriented siltstone rip-up clasts from underlying strata.
263 Paleomagnetic samples were oriented using a magnetic compass and a sun compass when-
264 ever possible. Sun compass data were preferentially used when available.

265 The specimens underwent step-wise thermal demagnetization in the UC Berkeley
266 Paleomagnetism Lab using an ASC demagnetizer (residual fields <10 nT) with measure-
267 ments of remanent magnetization made on a 2G DC-SQUID magnetometer. The demag-
268 netization protocol had increasingly high-resolution steps (5 to 2°C) approaching the Néel
269 temperature of hematite (up to ~687°C). Specimens were heated in the same relative
270 position within the thermal demagnetizer for each thermal demagnetization step. This
271 protocol was implemented to ensure similar relative temperature change for each sam-
272 ple during each heating step even in the presence of potential temperature gradients within
273 the oven. Implementing these high-resolution thermal demagnetization steps allowed us
274 to isolate magnetic remanence components carried by coarser detrital hematite grains
275 from finer pigmentary hematite grains (Fig. 4; Swanson-Hysell et al. (2019)). Least-squares
276 fits were made to distinct components (Kirschvink, 1980) using PmagPy (Tauxe et al.,
277 2016). All paleomagnetic data are available to the measurement level in the MagIC database
278 (<https://earthref.org/MagIC/19603/789b4868-fb73-4315-af37-81f599cacc4a>; this
279 link is for review purposes and will be updated when the manuscript is given a doi).

280 **4 Results and Interpretation**281 **4.1 Thermal demagnetization**

282 High-resolution thermal demagnetization on the Cut Face Sandstone reveals three
 283 magnetization components: a low-temperature component that typically unblocks up to
 284 200°C, a mid-temperature component that was typically removed up to 650°C, and a high-
 285 temperature component that was typically removed between 650°C and 687°C (Fig. 4).
 286 The high-temperature component can be recognized as unblocking over a narrower tem-
 287 perature range approaching the Néel temperature of hematite leading to an increased
 288 gradient in demagnetization vs. temperature – expressed as a “shoulder” in demagne-
 289 tization plots (Fig. 4). Given the potential for overlapping thermal unblocking spectra,
 290 we typically selected conservatively low upper temperature bounds for the mid-temperature
 291 component (e.g. 600°C) to limit it being pulled towards the high-temperature compo-
 292 nent. In the specimen demagnetization data, there is typically a shallowing of inclina-
 293 tion from the mid-temperature component to the high-temperature component (Fig. 4).
 294 The high unblocking temperature range for the high temperature component is consis-
 295 tent with the interpretation that it is held by hematite grains that have sizes >400 nm
 296 and have unblocking temperatures close to the Néel temperature of hematite (Jiang et
 297 al., 2015; Swanson-Hysell et al., 2019). We interpret the high-temperature component
 298 to be a detrital remanent magnetization (DRM) acquired at the time of Cut Face Creek
 299 Sandstone deposition. In contrast, the relatively lower unblocking temperatures and gen-
 300 erally steeper inclinations for the mid-temperature component is consistent with them
 301 being carried by pigmentary hematite grains of smaller sizes (<400 nm) that record a
 302 chemical remanent magnetization (CRM) during their growth within the sediment soon
 303 after deposition (Swanson-Hysell et al., 2019). Of the 179 samples analyzed from the Cut
 304 Face Creek Sandstone, a high-temperature component was resolved in 157 specimens,
 305 while a mid-temperature component was resolved in 167 specimens, and a low-temperature
 306 component in 109 specimens (Fig. 4).

307 Fisher statistics were calculated to obtain mean directions for each component. In
 308 geographic coordinates not corrected for bedding tilt, the mean low-temperature com-
 309 ponent has a declination of 359.3° and an inclination of 67.2° ($\alpha_{95}=2.0$; $k=46.0$; $n=109$;
 310 Fig. 4). This direction is indistinguishable from the local expected dipole field (dec=000.0°,
 311 inc=65.6°) consistent with it being a recently acquired viscous remanent magnetization.

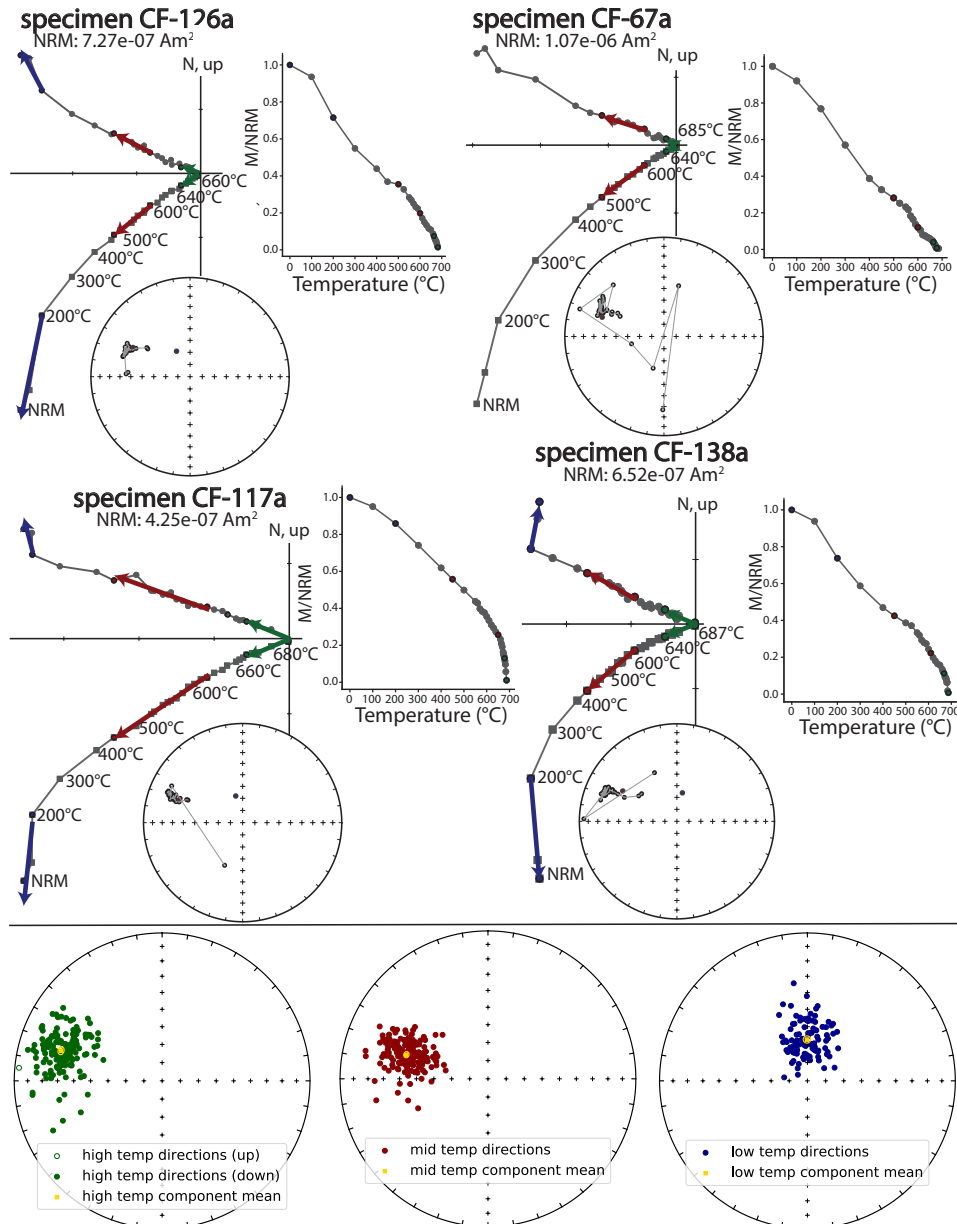


Figure 4: Example specimen thermal demagnetization results (top panel) and summary of all remanence components on equal area plots (bottom panel). The vector orthogonal plots show progressive magnetization direction changes through high-resolution demagnetization. The low-temperature component (blue) with a northerly declination and steep downward inclination is interpreted to have been acquired recently as its direction is indistinguishable from the present local axial dipole field. The mid-temperature component (red) is interpreted to be a chemical remanent magnetization (CRM) acquired soon after deposition of the Cut Face Creek Sandstone and was not flattened. The high temperature component (green) is interpreted as a detrital remanent magnetization (DRM) acquired through sediment deposition that was shallowed due to depositional and post-depositional processes.

312 The bedding tilt-corrected mid-temperature component has a mean declination of 286.5°
 313 and an inclination of 42.0° ($\alpha_{95}=1.6$; $k=48.2$; $n=167$). This direction is indistinguish-

able from the mean direction of the lava flows of the upper northeast sequence of the North Shore Volcanic Group ($\text{dec}=290.7^\circ$; $\text{inc}=41.4^\circ$ $\alpha_{95}=4.9^\circ$; $n=28$; Swanson-Hysell et al. (2019); Fig. 5) as they pass a statistical common mean test. This directional similarity is consistent with the interpretation that the pigmentary hematite grains within the Cut Face Creek Sandstone formed soon after deposition as a CRM and did not experience shallowing following formation. The tilt-corrected high-temperature component has a mean declination of 286.6° and an inclination of 29.4° ($\alpha_{95}=1.9^\circ$; $k=35.8$; $n=157$). The high-temperature component has a nearly identical mean declination with that of the mid-temperature component, but its mean inclination is shallower than that of the mid-temperature component and that of the lava flows (Fig. 5). In addition to a shallower mean inclination, the shape of the distribution is skewed such that directions are more elongate towards the horizontal plane consistent with sedimentary inclination flattening (Tauxe and Kent (2004); resulting in an elongation axis trending NE-SW for this data set; Fig. 4). This elongation contrasts with that of the mid-temperature component which is elongate in the vertical plane (an elongation axis trending NW-SE for this data set) as expected for an unflattened distribution of directions (Fig. 4). Taken together with the unblocking temperatures consistent with detrital hematite, the shallowed inclination and the distribution shape indicate that the high-temperature magnetization is a detrital remanent magnetization.

4.2 Empirical inclination shallowing assessment

Given that the true paleomagnetic direction at the time of Cut Face Creek Sandstone deposition can be constrained by the records of the bracketing North Shore Volcanic Group and the sandstone's CRM directions which are not shallowed (i.e. they share a common mean with the volcanic directions; Fig. 5A), we can empirically determine the degree of inclination shallowing of the DRM and compare the results with that from the statistical E/I method (Tauxe & Kent, 2004).

Given that there are uncertainties associated with each mean direction, there will be a range of f factors that will steepen the DRM direction to share a common mean with the directions that are not shallowed. To determine this range, we incrementally corrected all specimen DRM directions by an f factor ranging from 1 to 0 with a step size of 0.001 (Fig. 5). As f decreases from 1 to 0 (i.e. the amount of unflattening increases), it is observed that the angles between the mean direction of the corrected DRM direc-

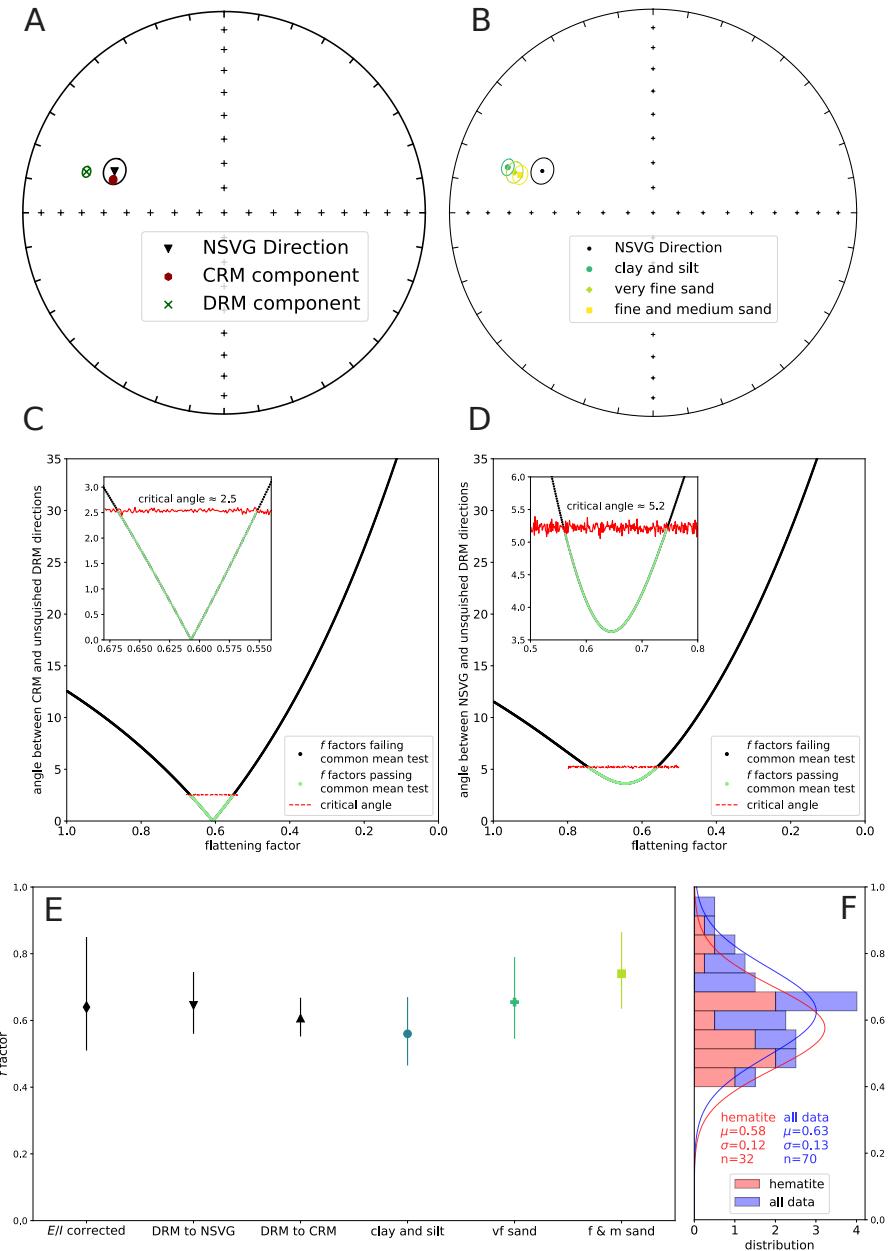


Figure 5: (A) Equal area plot comparing mean directions of Cut Face Creek Sandstone CRM and DRM magnetizations with that of the upper northeast sequence of the North Shore Volcanic Group (NSVG; Swanson-Hysell et al. (2019)). The mean CRM direction is indistinguishable from the volcanic direction while the DRM is shallowed relative to both. (B) Equal area plot comparing DRM directions of specimens grouped by grain size. Finer grain sizes have experienced more inclination shallowing. (C, D) Flattening factor estimates determined by progressively unflattening DRM directions and performing common mean tests between the DRM directions corrected by a given f factor and the CRM directions (in C) and the volcanics directions (in D). Green points are those that resulted in a statistically indistinguishable common mean (McFadden & McElhinny, 1990). The f factor resulting in the smallest angles and these common mean f factor test ranges for both DRM to NSVG volcanics and DRM to CRM are shown in (E) along with the f factor estimated using the E/I method and its associated 95% confidence bounds (Fig. 6). Also shown are the f factors and ranges for the DRM directions grouped by grain size compared to the NSVG directions. The stacked histogram in (F) summarizes compiled f factors for hematite-bearing sedimentary rocks (building on the compilations of Bilardello (2016) and Vaes et al. (2021)) as well as magnetite/mixed detrital magnetic mineralogy on the same axis as the estimates from this study in (E). A normal distribution fit to the f factors for hematite-bearing rocks has a mean of 0.58 with 1σ of 0.12. A normal distribution fit to magnetite and hematite data has a mean of 0.63 with 1σ of 0.13.

tions and those of both the CRM directions and the lava flow directions decrease toward a minimum when f is around 0.6, which is followed by an increase as the directions are steepened toward vertical (Fig. 5). In addition to calculating the angle between the mean of the corrected DRM directions and the means of the CRM and lava directions, we conducted common mean tests at each f factor (McFadden and McElhinny (1990); Fig. 5). In each iteration, the f factor is deemed plausible if the null hypothesis that the two populations share a common mean cannot be rejected. An f factor of 0.65 minimizes the angle between the DRM and the volcanic directions (3.6° angular difference) with the populations having statistically indistinguishable populations (i.e. passing a common mean test) between f factors of 0.75 and 0.56 (Fig. 5D). An f factor of 0.61 minimizes the angle between the DRM and CRM (0.01° angular difference) with statistically indistinguishable directions between 0.67 and 0.55 (Fig. 5C). These empirical f factors are similar (Fig. 5E) with the uncertainty of the f factor determined through the DRM to CRM comparison being smaller due to the higher number of vectors in the CRM population ($n=167$) than in the volcanics population ($n=28$).

As an additional analysis, we grouped the specimens by grain size and compared the specimen DRM directions to the volcanic directions. This analysis revealed claystone/siltstone to have been shallowed the most ($f = 0.56_{0.47}^{0.67}$), followed by the very fine-grained sandstones ($f = 0.66_{0.55}^{0.79}$), with the inclinations of specimens of medium- to fine-grained sandstone being the least shallowed ($f = 0.74_{0.64}^{0.87}$) (Fig. 5B,E).

4.3 Elongation/inclination flattening assessment

Applying the statistical E/I method to estimate the extent of inclination shallowing yielded an f factor of 0.64 with a 95% confidence range of 0.85 to 0.51 (Fig. 6). This uncertainty range is determined through 5,000 bootstrap resamples. The f factor estimate of $0.64_{0.51}^{0.85}$ obtained using the E/I method is very similar to that obtained empirically through the comparison of the DRM to the volcanics ($f = 0.65_{0.56}^{0.75}$) and the DRM to the CRM ($f = 0.61_{0.55}^{0.67}$) albeit with large associated uncertainty.

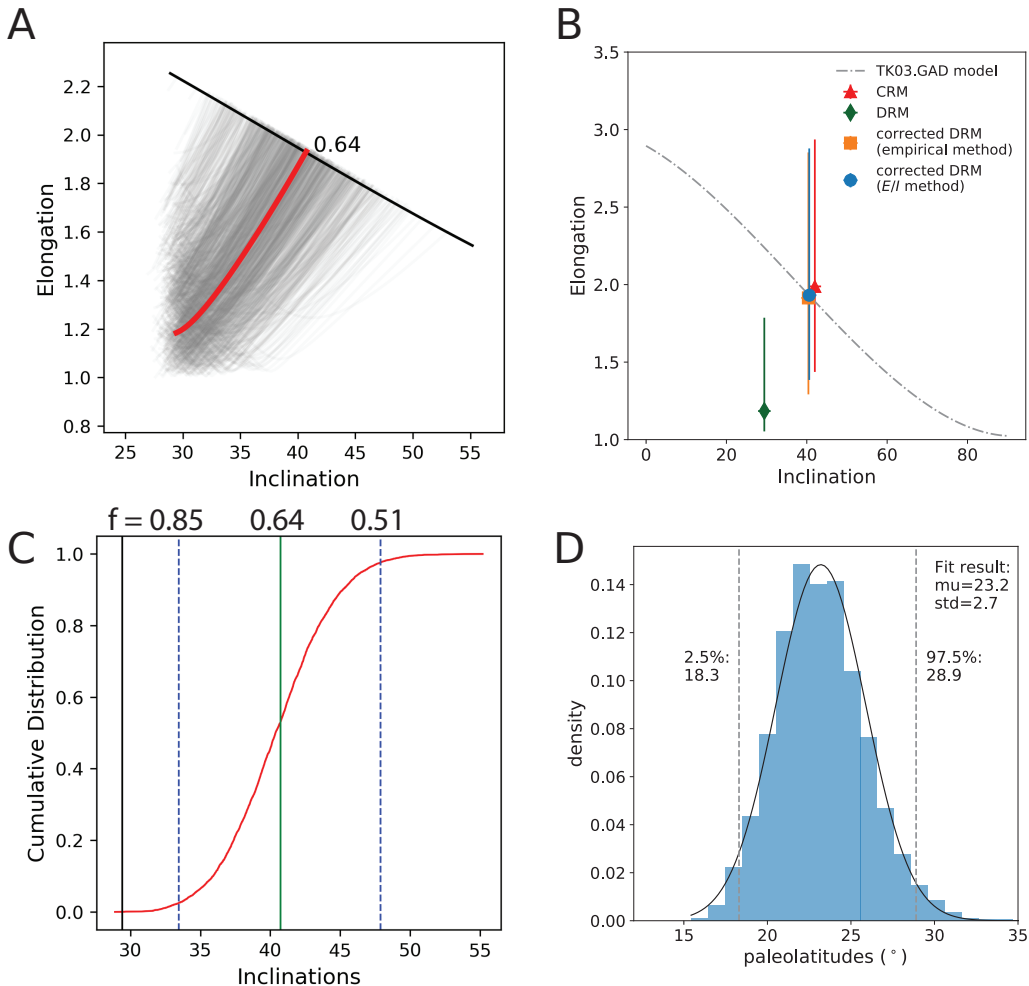


Figure 6: Results of the estimated amount of inclination shallowing of the detrital remanent magnetization of the Cut Face Creek sandstone using the elongation/inclination method (Tauxe & Kent, 2004). (A) The E/I method results in an estimated flattening factor of $f=0.64$ (red curve) based on where elongation/inclination intersects that predicted by the TK03 paleosecular variation model (black curve). The grey lines show the analysis applied to 5,000 bootstrap resamples of the DRM directions of the Cut Face Creek Sandstone which provide an estimate of the uncertainty associated with the f factor estimate. To explore the effect of convolving DRM and CRM components, this same analysis is conducted on fits where these components are not separated in the Supporting Information in Fig. S2. B) The distribution of the CRM vectors (red triangle) as well as those for the DRM corrected with $f=0.65$ (value that minimize the angle between the mean of the corrected DRM and the mean pole of the NSVG lava flows; orange square) have E/I values that are very close to that predicted by TK03.GAD. The DRM vectors corrected by the E/I method (blue circle) are directly on the TK03.GAD curve by definition of the method. C) The cumulative distribution of all plausible inclinations based on the E/I bootstrap results. D) The distribution of the paleolatitudes implied from the inclinations that result from the E/I method bootstrap resamples. The 95% confidence range spans a range of paleolatitudes that needs to be incorporated into the uncertainty on the resulting paleomagnetic pole.

373

5 Discussion

374

5.1 Inclination shallowing in hematite-bearing sedimentary rocks

375

As has been long demonstrated in experimental and field studies (e.g. Tauxe & Kent, 1984; Lovlie & Torsvik, 1984), our study found that the remanence held by detrital hematite

376

377 was shallowed with respect to the field in which it was acquired. In contrast, the rema-
 378 nence held by pigmentary hematite recovered the expected direction. The rapid accu-
 379 mulation of subsequent lava flows within the North Shore Volcanic Group may have ac-
 380 celerated the chemical transformation to pigmentary hematite of precursor iron oxide
 381 phases such as ferrihydrite such that it occurred soon (<1 Myr) after deposition. In this
 382 case, it is both interesting and useful that the CRM held by the pigmentary hematite
 383 returns the expected direction. However, since it is inherently a secondary phase that
 384 could be acquired on varied timescales, we caution against this result being broadly ex-
 385 trapolated to other formations. As was found in the study of siltstone intraclasts by Swanson-
 386 Hysell et al. (2019), high-resolution thermal demagnetization steps are necessary to iso-
 387 late the DRM from the CRM. Isolating DRM held by detrital hematite is quite impor-
 388 tant if one is then applying an inclination flattening correction given that the CRM of
 389 pigmentary hematite is not expected to be flattened as shown in this study.

390 The f factors determined in this study of $f = 0.65^{0.75}_{0.56}$ for the comparison of the
 391 DRM to the volcanics, $f = 0.61^{0.67}_{0.55}$ for the comparison of the DRM to the CRM, and
 392 $0.64^{0.85}_{0.51}$ through the E/I method are all similar to one another (Fig. 5E). In addition,
 393 they overlap with compiled f factors in the literature for hematite-bearing sedimentary
 394 rocks (Fig. 5F). One approach that has been taken in the literature is to assume an f
 395 factor of 0.6 and apply that to sedimentary poles for which no study specific factor was
 396 determined (Domeier et al., 2012; Torsvik et al., 2012). This assumed value was informed
 397 through a compilation of f factors developed using anisotropy approaches and the E/I
 398 method that was presented in Bilardello and Kodama (2010c). The f factor determined
 399 empirically for the Cut Face Creek Sandstone in this study is quite close to the assumed
 400 value of 0.6 applied to sedimentary paleomagnetic data by (Torsvik et al., 2012). How-
 401 ever, numerous studies (e.g. Bilardello and Kodama (2010c) and Ding et al. (2015)) have
 402 cautioned against applying an assumed f factor and the variability in f factors between
 403 formations and within individual formations continues to be highlighted as inconsistent
 404 with a single value (e.g. Vaes et al., 2021). Our data corroborate this perspective as they
 405 reveal a relationship where the finer grained clay and siltstone lithologies are more flat-
 406 tened than the sandstone lithologies highlighting the variability of flattening in clastic
 407 sedimentary rocks as discussed in more detail below (Fig. 5).

408 **5.2 Implications for applying the TK03 model and the *E/I* method in**
 409 **deep time**

410 The TK03 model for paleosecular variation, and therefore the target inclination-
 411 elongation curve that is used in the *E/I* method, was developed to match the variation
 412 of scatter within a compilation of lava flows for the past 5 Myr (McElhinny & McFad-
 413 den, 1997; Tauxe & Kent, 2004). It remains an open question whether this model is rep-
 414 resentative of the field at times further back in Earth history. There is support that comes
 415 from compilations of data from large igneous provinces over the Phanerozoic Era, and
 416 back to the 1.1 Ga Midcontinent Rift, that yield inclination-elongation relationships con-
 417 sistent with that predicted by the model (Tauxe et al., 2008; Tauxe & Kodama, 2009).
 418 Additionally, comparisons between sedimentary inclinations corrected through the *E/I*
 419 method and coeval volcanics have been shown to yield consistent results in multiple stud-
 420 ies including ca. 200 Ma (Kent & Olsen, 2008) and ca. 50 Ma (Vaes et al., 2021).

421 In our study, the close correspondence of the *f* factor determined through the *E/I*
 422 method and the empirical approach (Fig. 5E) supports the application of *E/I* at this
 423 time in the late Mesoproterozoic Era (the Stenian Period). A caveat to this conclusion
 424 is that there is large uncertainty on the *f* factor coming out of the bootstrap analysis
 425 as is typical when applying the *E/I* method to paleomagnetic data sets which limits the
 426 precision of the comparison. These uncertainties arise from the the reality that the shape
 427 of a distribution is more uncertain and prone to variability through bootstrap resampling
 428 than the mean of a distribution.

429 Another way to evaluate the applicability of the TK03 model in the late Mesopro-
 430 terozoic is to consider the shape of the distribution of CRM directions (Fig. 6). These
 431 directions represent unflattened magnetization acquired as pigmentary hematite was grow-
 432 ing within the sediment following deposition from precursor ferric oxide phases. The re-
 433 lationship of the elongation and the unflattened inclination recorded by the pigmentary
 434 hematite corresponds closely with that of the TK03.GAD model (Fig. 6B). While there
 435 is appreciable uncertainty on the elongation estimate through this analysis (as represented
 436 in the bootstrap determined confidence bounds in Fig. 6B), it provides additional sup-
 437 port for applying the TK03.GAD model in deep time.

438 **5.3 Uncertainty in flattening factor estimates**

439 Uncertainty is inherent to any method of estimating a flattening factor. Even in
 440 the case of an empirical flattening analysis with comparison to well-constrained unflat-
 441 tened time-equivalent directions as in this study, the uncertainty on mean directions leads
 442 to a range of plausible f factors (as determined through the common mean tests shown
 443 in Fig. 5). This range is more dramatic when the E/I method is applied given the lim-
 444 itations in tightly constraining the shape of a distribution from a population of vectors
 445 at a number that is feasible to obtain through paleomagnetic study. Correcting the DRM
 446 directions by the f values of 0.85 and 0.51 at the bounds of the 95% confidence inter-
 447 val found through E/I analysis (Fig. 6) will result in two distinct direction distributions
 448 (i.e. they fail a common mean test) whose mean directions are 13.3° apart. Such an an-
 449 gular difference in directional space translates into a 9.7° difference in calculated pole
 450 positions for the Cut Face Creek Sandstone. This difference highlights that such uncer-
 451 tainty on inclination needs to be incorporated into mean paleomagnetic poles developed
 452 from sedimentary rocks.

453 In addition to data analysis challenges which lead to inescapable uncertainty, there
 454 is also the reality that a sedimentary unit will have varying flattening factors in differ-
 455 ent horizons. Variability in ferromagnetic mineral assemblages, sedimentary grain size,
 456 and depositional processes—all of which are expected within a sedimentary formation—
 457 will impact flattening. The variability in inclination shallowing as a function of grain size
 458 has been shown in redeposition experiments such as those conducted by Tan et al. (2002)
 459 on disaggregated red beds. Their finding that deposits of finer grain size are more prone
 460 to inclination shallowing is consistent with our finding of shallower inclination in siltstone
 461 than very fine sandstone which in turn is more shallowed than fine to medium sandstone
 462 (Fig. 5B).

463 Despite expected variability in flattening factors within a single sedimentary rock
 464 unit and inherent uncertainty in methods of determining f factors, studies typically use
 465 a single f factor to correct for inclination shallowing. This approach holds true both in
 466 studies that assume a single f factor (e.g. 0.6 applied to all sedimentary poles; Torsvik
 467 et al. (2012)) as well as in studies that develop estimates through anisotropy approaches
 468 or the E/I method both of which have associated uncertainty. In the case of the E/I
 469 method, researchers often consider the resulting f factor but do not incorporate the as-

470 associated bootstrap uncertainty bounds when interpreting the data and developing as-
 471 sociated paleomagnetic poles.

472 **5.4 Better representing inclination shallowing uncertainties in sedimentary paleomagnetic poles**

473 Given that there is uncertainty in f factor regardless of method, this uncertainty
 474 needs to be incorporated into the uncertainty on the mean pole position developed from
 475 detrital remanent magnetization in sedimentary rocks. While paleomagnetic poles are
 476 typically represented by circularly symmetric Fisher distributions, uncertainty in f fac-
 477 tor will increase uncertainty in the direction between an unflattened paleomagnetic pole
 478 and the study site such that the spherical uncertainty region is elliptical.
 479

480 A strength of the E/I method is that the bootstrap approach to determine uncer-
 481 tainty returns an ensemble of f factors that represents the uncertainty on the inclina-
 482 tion correction. In Figure 6D, we show the distribution of paleolatitudes that results from
 483 applying these f factors to variably correct the shallowed Cut Face Creek Sandstone DRM.
 484 The resulting paleolatitude distribution can be approximated by a normal distribution
 485 (mean=23.2°N; one standard deviation=2.7°; Fig. 6D). A Kent distribution implements
 486 a bivariate normal distribution on a sphere which can therefore represent increased un-
 487 certainty in the colatitude direction (the conjugate of paleolatitude) between the study
 488 site and the paleomagnetic pole. The distribution shown in Fig. 6D has a heavy tail given
 489 the transformation of directions to pole space such that representation with a normal
 490 distribution is an approximation. However this is a useful approximation, as the Kent
 491 distribution provides a succinct way to summarize the uncertainties associated with sed-
 492 imimentary paleomagnetic poles that include f factor uncertainty.

493 To determine this uncertainty, we took all of the f factors from the E/I analysis
 494 (with 5,000 bootstrap resamples) and applied them to the DRM directions (Fig. 7A).
 495 Note that this can alternatively be done with a distribution of f factors associated with
 496 anisotropy uncertainty or from a compilation as discussed further below. Such a boot-
 497 strap resampling approach was applied in Bilardello et al. (2011) to parameters associ-
 498 ated with anisotropy estimates and propagated into site mean directional data. For each
 499 f factor from the E/I analysis, we converted the directions to virtual geomagnetic poles
 500 (VGPs; grey in Fig. 7B) and calculated the mean paleomagnetic pole at each f factor

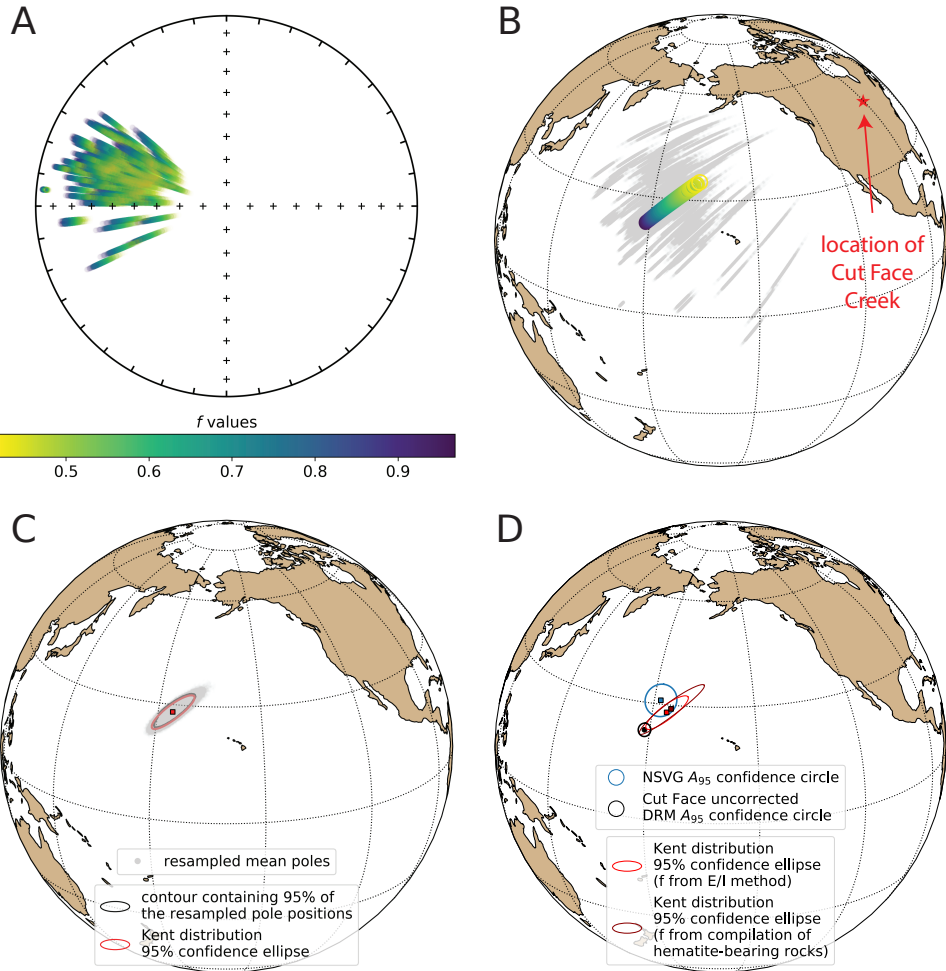


Figure 7: A new method for incorporating inclination shallowing uncertainty into sedimentary paleomagnetic poles. With each of the 5,000 f values determined from the E/I method bootstrap resampling routine (Tauxe & Kent, 2004), we corrected all Cut Face Creek Sandstone DRM directions (shown colored by f factor in (A) and calculated their associated virtual geomagnetic pole positions (grey points in B). Mean pole positions with associated A_{95} calculated with Fisher statistics are shown in (B) also color-coded by the f factor that leads to that pole. To characterize the distribution shape, we Monte-Carlo resampled 100 random inclination-corrected mean pole positions from the angular standard deviation (θ_{95}) of the Fisher mean pole associated with each f value. The total 500,000 Monte-Carlo resampled results on the mean pole positions are shown as grey points in (C) along with the contour that encapsulates 95% of the resampled mean poles (in black). Also shown is the 95% confidence ellipse of the Kent distribution (red ellipse) which closely matches the 95% contour indicating that it is an effective summary of the distribution. The Kent distribution confidence ellipse for the Cut Face Creek pole that includes the f factor uncertainty resulting from the E/I method is shown in comparison with the North Shore Volcanic Group (NSVG) Fisher mean pole position in (D). Also shown is the Kent distribution that results from applying the same approach with bootstrap resampled f factors taken from a compilation of published values. This approach could be applied to estimate the uncertainty of published sedimentary poles where E/I analysis is not possible.

as a Fisher mean (colored by f factor in Fig. 7B). What would typically be done with a single f factor (either calculated or assumed) is to take a single one of these poles as

the resulting pole and report its Fisher mean which would underestimate uncertainty along the great circle between the pole and the study locality. Instead, we have an ensemble of possible poles associated with the ensemble of f factors. From these poles, we drew 100 random pole mean positions from each of the Fisher-distributed mean poles (grey poles in Fig. 7C). These resampled poles represent 500,000 possible mean pole positions and their elliptical distribution can be seen with the contour that contains 95% of the resampled mean pole positions (black curve in Fig. 7C). A Kent distribution calculated from these resampled mean poles that incorporates the flattening uncertainty is shown in red in Figure 7C and is very similar to the 95% contour. Kent distributions can be reported as the mean direction (γ_1), the major axis (γ_2) with a 95% semi-angle (ζ_{95}), and the minor axis (γ_3) with a 95% semi-angle confidence angle (η_{95}). The ellipse has its major axis along the great circle between γ_1 and γ_2 with its minor axis along the great circle between γ_1 and γ_3 . The Kent mean ellipse for the Cut Face Creek Sandstone incorporating flattening uncertainty from the E/I method has a mean of Plon=184.4°E, Plat = 28.1°N, a major axis of $\gamma_2=[297.9^{\circ}\text{E}, 36.7^{\circ}\text{N}]$ with a semi-angle of $\zeta_{95}=6.7^{\circ}$ and a minor axis of $\gamma_3=[67.3^{\circ}\text{E}, 40.4^{\circ}\text{N}]$ with a semi-angle of $\eta_{95}=1.8^{\circ}$. The inclination corrected DRM Kent mean pole overlaps with the Fisher mean pole for the volcanics (Fig. 7).

For published datasets without estimates of inclination shallowing, one approach to incorporate the uncertainty associated with inclination shallowing is to use f factors from a compilation in contrast to assuming a single value (Bilardello & Kodama, 2008, 2009). Building on the compilations of Bilardello (2016) and Vaes et al. (2021), we compiled f factors from both anisotropy and E/I methods from clastic sedimentary rocks (Table S1). This compilation is summarized in the histogram in Figure 5F and Figure S1. The compilation reveals similar means and distributions between detrital magnetic mineralogies with slightly lower f values for hematite (Fig. 5F and Fig. S1). If an ensemble of f factors resulting from the EI method is not available for a sedimentary paleomagnetic pole, these compiled f factors could be used to estimate the uncertainty associated with inclination shallowing and develop a Kent distribution pole. To do so, we follow the same approach described above with the modification of using f factors that are drawn from bootstrap resampling from the compilation. As is visualized in Figure 7D, the resulting uncertainty ellipse is larger than that when f factors come from the E/I analysis given that our knowledge of the inclination shallowing is less informed and

Table 1: Kent mean paleomagnetic poles for the Cut Face Creek Sandstone

pole	mean pole	major axis	major axis	minor axis	minor axis
	position	95% confidence		95% confidence	
	(Plon/Plat)	angle	angle		
	γ_1	γ_2	ζ_{95}	γ_2	η_{95}
Cut Face <i>E/I</i>	184.4°E /	297.9°E /	6.7°	67.3°E /	1.8°
corrected	28.1°N	36.7°N		40.4°N	
Cut Face compilation	185.7°E /	299.8°E /	10.8°	67.6°E /	1.7°
	29.3°N	36.0°N		40.1°N	
corrected					

Notes: The Fisher mean of the Cutface Creek paleomagnetic pole without an inclination
shallowing correction is Plon=178.5, Plat=23.0, A₉₅=1.7; the values associated with the
compilation correction can slightly change with different bootstrap resampling runs given
the relatively low number of *f* factors in the compilation.

taken from all estimated *f* factors. The Kent means and associated statistics resulting
from applying the *E/I* correction and the compilation-based correction to the Cut Face
Creek Sandstone are summarized in Table 1. Applying this method to synthetic and other
sedimentary datasets yields similarly reasonable results as shown in the archived Jupyter
notebooks accompanying this work.

A future direction to explore is the assignment of distinct *f* factors to different por-
tions of a sedimentary succession based on characteristics such as grain size. With suf-
ficient numbers of directions, one approach could be to apply E/I analysis on data sep-
arated by grain size within a formation from which the *f* factor distributions are then
resampled for pole uncertainty estimation. A similar grouping approach could be taken
using the compilation method. Selecting distinct *f* factors for different portions of a sed-
imentary succession could have the effect of reducing the estimated uncertainty on a re-
sulting paleomagnetic pole. Instead of the maximum and minimum *f* factors being ap-

plied uniformly to all specimen directions, resampled f factors from different populations could lead to a spread of f that moderate the overall spread in possible VGP positions.

Incorporating inclination shallowing uncertainty into the presentation of mean paleomagnetic poles has several advantages. It more completely communicates the uncertainty associated with paleomagnetic poles developed from detrital remanent magnetization. Fisher mean paleomagnetic poles developed from sedimentary data often have small circular A_{95} confidence ellipses due to large numbers of samples in the mean. However, these small A_{95} uncertainty angles overestimate the confidence on the known position—particularly the co-latitude. Representing the uncertainty has the potential to reconcile disparate poles and address paleogeographic puzzles. Being able to approximate the mean pole position as a Kent distribution enables the mean pole and the uncertainty to be succinctly communicated. Additionally, the Kent distribution can be incorporated into frameworks such that probabilistic inversion or parametric Monte Carlo resampling can enable development of future apparent polar wander paths that incorporate uncertainty.

6 Conclusion

The Cut Face Creek Sandstone provides a 1.1-billion-year-old natural laboratory where the paleomagnetic pole position expected to have been recorded by the red beds can be tightly constrained by the lava flows that bracket it such that the amount of inclination shallowing of the sediments can be empirically determined. The statistical E/I method (Tauxe & Kent, 2004) yields an estimated range of f values for the hematite detrital remanent magnetization that agree with those derived empirically, but with larger uncertainties. Given that all methods have non-negligible uncertainties associated with determining the flattening factor, they should be recognized and incorporated into paleomagnetic syntheses. Incorporating uncertainty associated with inclination flattening leads to increased uncertainty in pole position between the unflattened pole position and the study site. We present a method that takes a range of unflattening factors and uses it to develop a mean pole and uncertainty ellipse that can be approximated as a Kent distribution. This method can be applied to datasets where f factors have been determined through E/I analysis as well as to datasets without such determination in which case the range of f factors can be taken from a literature compilation. Incorporating inclination shallowing uncertainty better represents our knowledge of ancient paleomagnetic pole positions thereby advancing paleogeographic reconstructions.

581 7 Open research

582 Paleomagnetic data associated with this study are available within the MagIC database
583 (<https://doi.org/10.7288/V4/MAGIC/19603>) and all data are within a Github repos-
584 itory associated with this work (https://github.com/Swanson-Hysell-Group/Inclination_Shallowing) that is also archived on Zenodo (<https://doi.org/10.5281/zenodo.7201226>).
585 This repository also contains Python code that implements all of the calculations, vi-
586 sualizations and statistical tests discussed herein. We added to the Pmagpy Python pack-
587 age (Tauxe et al., 2016) a new function named *find_ei_kent* that finds the estimated range
588 of plausible inclination shallowing factors for a set of sedimentary paleomagnetic direc-
589 tions using the *E/I* method and returns the associated Kent distribution that includes
590 the uncertainty estimates from the *E/I* method to estimate the 95% confidence ellipse
591 for a sedimentary paleomagnetic pole.
592

593 Acknowledgments

594 Support for this research came from NSF grant EAR-1847277 to Nicholas Swanson-Hysell
595 and an UC Berkeley Summer Undergraduate Research Fellowship awarded to James Pierce.
596 Lisa Tauxe provided inspiration and feedback on the approach taken in this study. Mar-
597 garet Avery provided feedback on an earlier draft of the manuscript. Sarah Swanson-
598 Hysell and Madeline Swanson-Hysell assisted with fieldwork. Dario Bilardello provided
599 a curated compilation of *f* factors associated with Bilardello (2016) that he updated to
600 include more recent data for the talk “The Anisotropy Correction for Inclination Shal-
601 lowing” presented at the 2021 Institute for Rock Magnetism Conference. He also pro-
602 vided insightful conversation related to inclination shallowing and his contributions to
603 the field. We appreciate thoughtful reviews of the manuscript from Ken Kodama and
604 Mat Domeier as well as the editorial handling of Josh Feinberg.

605 **References**

- Anson, G. L., & Kodama, K. P. (1987). Compaction-induced inclination shallowing of the post-depositional remanent magnetization in a synthetic sediment. *Geophysical Journal International*, 88(3), 673–692.
- Bazhenov, M. L., & Shatsillo, A. V. (2010). Late Permian palaeomagnetism of Northern Eurasia: data evaluation and a single-plate test of the geocentric axial dipole model. *Geophysical Journal International*, 180(1), 136–146. doi: 10.1111/j.1365-246x.2009.04379.x
- Bilardello, D. (2015). Isolating the anisotropy of the characteristic remanence-carrying hematite grains: a first multispecimen approach. *Geophysical Journal International*, 202(2), 695–712. doi: 10.1093/gji/ggv171
- Bilardello, D. (2016). The do's and don'ts of inclination shallowing corrections. *The IRM Quarterly*, 26(3), 12.
- Bilardello, D., Callebert, W. C., & Davis, J. R. (2018). Evidence for widespread remagnetizations in South America, case study of the Itararé Group rocks from the state of São Paulo, Brazil. *Frontiers in Earth Science*, 6. doi: 10.3389/feart.2018.00182
- Bilardello, D., Jezek, J., & Kodama, K. P. (2011). Propagating and incorporating the error in anisotropy-based inclination corrections. *Geophysical Journal International*, 187(1), 75–84. doi: 10.1111/j.1365-246x.2011.05138
- Bilardello, D., & Kodama, K. (2008). A simplified red bed inclination correction: A case study from the Permian Esterel Rocks of France. In *American Geophysical Union* (p. GP51A-0733).
- Bilardello, D., & Kodama, K. (2009). Magnetic fabric and inclination shallowing studies: depositional and post-depositional processes in hematite- and magnetite-bearing rocks. In *American Geophysical Union* (p. GP43A-0841).
- Bilardello, D., & Kodama, K. P. (2010a). A new inclination shallowing correction of the Mauch Chunk Formation of Pennsylvania, based on high-field AIR results: Implications for the Carboniferous North American APW path and Pangea reconstructions. *Earth and Planetary Science Letters*, 299(1-2), 218–227. doi: 10.1016/j.epsl.2010.09.002
- Bilardello, D., & Kodama, K. P. (2010b). Palaeomagnetism and magnetic anisotropy of Carboniferous red beds from the Maritime Provinces of Canada: evidence

- for shallow palaeomagnetic inclinations and implications for North American apparent polar wander. *Geophysical Journal International*, 180(3), 1013–1029. doi: 10.1111/j.1365-246X.2009.04457.x
- Bilardello, D., & Kodama, K. P. (2010c). Rock magnetic evidence for inclination shallowing in the early Carboniferous Deer Lake Group red beds of western Newfoundland. *Geophysical Journal International*, 181(1), 275–289. doi: 10.1111/j.1365-246X.2010.04537.x
- Books, K. (1972). *Paleomagnetism of Some Lake Superior Keweenawan Rocks*. Geological Survey Professional Paper 760.
- Butler, R. F. (1992). *Magnetic Domains to Geologic Terranes*. Blackwell Scientific Publications.
- Cant, D. J., & Walker, R. G. (1976). Development of a braided-fluvial facies model for the Devonian Battery Point Sandstone, Québec. *Canadian Journal of Earth Sciences*, 13(1), 102–119. doi: 10.1139/e76-010
- Chen, W., Zhang, S., Ding, J., Zhang, J., Zhao, X., Zhu, L., ... Wu, H. (2017). Combined paleomagnetic and geochronological study on Cretaceous strata of the Qiangtang terrane, central Tibet. *Gondwana Research*, 41, 373–389. doi: 10.1016/j.gr.2015.07.004
- Costa, E., Garces, M., López-Blanco, M., Beamud, E., Gómez-Paccard, M., & Larrasoña, J. C. (2009). Closing and continentalization of the South Pyrenean foreland basin (NE Spain): magnetochronological constraints. *Basin Research*. doi: 10.1111/j.1365-2117.2009.00452.x
- Dallanave, E., Kirscher, U., Hauck, J., Hesse, R., Bachtadse, V., & Wortmann, U. G. (2018). Palaeomagnetic time and space constraints of the Early Cretaceous Rhenodanubian Flysch zone (Eastern Alps). *Geophysical Journal International*, 213(3), 1804–1817. doi: 10.1093/gji/ggy077
- Deenen, M. H. L., Langereis, C. G., van Hinsbergen, D. J. J., & Biggin, A. J. (2011). Geomagnetic secular variation and the statistics of palaeomagnetic directions. *Geophysical Journal International*. doi: 10.1111/j.1365-246X.2011.05050.x
- Ding, J., Zhang, S., Chen, W., Zhang, J., Yang, T., Jiang, G., ... Wu, H. (2015). Paleomagnetism of the Oligocene Kangtuo Formation red beds (Central Tibet): Inclination shallowing and tectonic implications. *Journal of Asian Earth Sciences*

- 671 *Sciences*, 104, 55–68. doi: 10.1016/j.jseae.2014.10.006

672 Domeier, M., Van der Voo, R., & Torsvik, T. H. (2012). Paleomagnetism and
673 Pangea: The road to reconciliation. *Tectonophysics*, 514–517, 14–43. doi:
674 10.1016/j.tecto.2011.10.021

675 Driscoll, P. E., & Evans, D. A. (2016, March). Frequency of Proterozoic geomag-
676 netic superchrons. *Earth and Planetary Science Letters*, 437, 9–14. Re-
677 trieval 2022-02-15, from <https://linkinghub.elsevier.com/retrieve/pii/S0012821X15007980> doi: 10.1016/j.epsl.2015.12.035

679 Dupont-Nivet, G., Lippert, P. C., Hinsbergen, D. J. V., Meijers, M. J., & Kapp,
680 P. (2010). Palaeolatitude and age of the Indo-Asia collision: palaeomag-
681 netic constraints. *Geophysical Journal International*, 182(3), 1189–1198. doi:
682 10.1111/j.1365-246x.2010.04697.x

683 Gallo, L. C., Tomezzoli, R. N., & Cristallini, E. O. (2017). A pure dipole analysis
684 of the Gondwana apparent polar wander path: Paleogeographic implications
685 in the evolution of Pangea. *Geochemistry, Geophysics, Geosystems*, 18(4),
686 1499–1519. doi: 10.1002/2016gc006692

687 Green, J. C. (1983). Geologic and geochemical evidence for the nature and devel-
688 opment of the middle Proterozoic (Keweenawan) Midcontinent Rift of North
689 America. *Tectonophysics*, 94(1), 413–437. doi: 10.1016/0040-1951(83)90027-6

690 Green, J. C., Boerboom, T. J., Schmidt, S. T., & Fitz, T. J. (2011). The North
691 Shore Volcanic Group: Mesoproterozoic plateau volcanic rocks of the Midcon-
692 tinent Rift system in northeastern Minnesota. *Archean to Anthropocene: Field*
693 *Guides to the Geology of the Mid-Continent of North America: Geological*
694 *Society of America Field Guide*, 24, 121–146.

695 Gutiérrez, L., Barrón, V., Andrés-Vergés, M., Serna, C. J., Veintemillas-Verdaguer,
696 S., Morales, M. P., & Lázaro, F. J. (2016). Detailed magnetic monitoring
697 of the enhanced magnetism of ferrihydrite along its progressive transforma-
698 tion into hematite. *Journal of Geophysical Research: Solid Earth*, 121(6),
699 4118–4129. doi: 10.1002/2016JB013016

700 Haldan, M. M., Langereis, C. G., Biggin, A. J., Dekkers, M. J., & Evans, M. E.
701 (2009). A comparison of detailed equatorial red bed records of secular varia-
702 tion during the Permo-Carboniferous Reversed Superchron. *Geophysical Jour-*
703 *nal International*, 177(3), 834–848. doi: 10.1111/j.1365-246x.2009.04124.x

- 704 Huang, W., Dupont-Nivet, G., Lippert, P. C., van Hinsbergen, D. J. J., & Hallot,
 705 E. (2013). Inclination shallowing in Eocene Linzizong sedimentary rocks from
 706 Southern Tibet: correction, possible causes and implications for reconstructing
 707 the India–Asia collision. *Geophysical Journal International*, *194*(3), 1390–1411.
 708 doi: 10.1093/gji/ggt188
- 709 Huang, W., van Hinsbergen, D. J., Maffione, M., Orme, D. A., Dupont-Nivet, G.,
 710 Guilmette, C., ... Kapp, P. (2015). Lower Cretaceous Xigaze ophiolites
 711 formed in the Gangdese forearc: Evidence from paleomagnetism, sediment
 712 provenance, and stratigraphy. *Earth and Planetary Science Letters*, *415*,
 713 142–153. doi: 10.1016/j.epsl.2015.01.032
- 714 Jackson, M. J., Banerjee, S. K., Marvin, J. A., Lu, R., & Gruber, W. (1991). De-
 715 trital remanence, inclination Errors, and anhysteretic remanence anisotropy:
 716 Quantitative model and experimental results. *Geophysical Journal Interna-*
 717 *tional*, *104*(1), 95–103. doi: 10.1111/j.1365-246X.1991.tb02496.x
- 718 Jiang, Z., Liu, Q., Dekkers, M. J., Tauxe, L., Qin, H., Barrón, V., & Torrent, J.
 719 (2015). Acquisition of chemical remanent magnetization during experimental
 720 ferrihydrite–hematite conversion in Earth-like magnetic field—implications for
 721 paleomagnetic studies of red beds. *Earth and Planetary Science Letters*, *428*,
 722 1–10. doi: 10.1016/j.epsl.2015.07.024
- 723 Jiang, Z., Liu, Q., Roberts, A. P., Barrón, V., Torrent, J., & Zhang, Q. (2018). A
 724 new model for transformation of ferrihydrite to hematite in soils and sedi-
 725 ments. *Geology*. doi: 10.1130/G45386.1
- 726 Jiang, Z., Liu, Q., Roberts, A. P., Dekkers, M. J., Barrón, V., Torrent, J., & Li, S.
 727 (2022). The magnetic and color reflectance properties of hematite: From Earth
 728 to Mars. *Reviews of Geophysics*, *60*(1). doi: 10.1029/2020rg000698
- 729 Jirsa, M. A. (1984). Interflow Sedimentary Rocks in the Keweenawan North Shore
 730 Volcanic Group, Northeastern Minnesota. *Minnesota Geological Survey*, *28*.
- 731 Kent, D. V., & Olsen, P. E. (2008). Early Jurassic magnetostratigraphy and pale-
 732 olatitudes from the Hartford continental rift basin (eastern North America):
 733 Testing for polarity bias and abrupt polar wander in association with the
 734 central Atlantic magmatic province. *Journal of Geophysical Research: Solid*
 735 *Earth*, *113*(B6). doi: doi.org/10.1029/2007JB005407
- 736 Kent, D. V., & Tauxe, L. (2005). Corrected late triassic latitudes for continents ad-

- 737 jacent to the north atlantic. *Science*, 307(5707), 240–244. doi: 10.1126/science
 738 .1105826
- 739 Kim, B., & Kodama, K. P. (2004). A compaction correction for the paleomagnetism
 740 of the Nanaimo Group sedimentary rocks: Implications for the Baja British
 741 Columbia hypothesis. *Journal of Geophysical Research: Solid Earth*, 109(B2).
 742 doi: 10.1029/2003jb002696
- 743 King, R. F. (1955). The remanent magnetism of artificially deposited sediments.
 744 *Geophysical Supplements to the Monthly Notices of the Royal Astronomical
 745 Society*, 7(3), 115–134. doi: 10.1111/j.1365-246X.1955.tb06558.x
- 746 Kirscher, U., Bilardello, D., Mikolaichuk, A., & Bachtadse, V. (2014). Correcting for
 747 inclination shallowing of early Carboniferous sedimentary rocks from Kyrgyzs-
 748 tan—indication of stable subtropical position of the North Tianshan Zone in
 749 the mid-late Palaeozoic. *Geophysical Journal International*, 198(2), 1000–1015.
 750 doi: 10.1093/gji/ggu177
- 751 Kirschvink, J. L. (1980). The least-squares line and plane and the analysis of palaeo-
 752 magnetic data. *Geophysical Journal International*, 62(3), 699–718. doi: 10
 753 .1111/j.1365-246X.1980.tb02601.x
- 754 Kodama, K. P. (2009). Simplification of the anisotropy-based inclination cor-
 755 rection technique for magnetite- and haematite-bearing rocks: a case study
 756 for the Carboniferous Glenshaw and Mauch Chunk Formations, North
 757 America. *Geophysical Journal International*, 176(2), 467–477. doi:
 758 10.1111/j.1365-246x.2008.04013.x
- 759 Kodama, K. P. (2012). *Paleomagnetism of sedimentary rocks: process and interpre-
 760 tation*. Chichester, West Sussex ; Hoboken, NJ: John Wiley & Sons.
- 761 Kodama, K. P., & Davi, J. M. (1995). A compaction correction for the paleomag-
 762 netism of the Cretaceous Pigeon Point Formation of California. *Tectonics*,
 763 14 (5), 1153–1164. doi: 10.1029/95tc01648
- 764 Krijgsman, W., & Tauxe, L. (2004). Shallow bias in Mediterranean paleomagnetic
 765 directions caused by inclination error. *Earth and Planetary Science Letters*,
 766 222(2), 685–695. doi: 10.1016/j.epsl.2004.03.007
- 767 Krijgsman, W., & Tauxe, L. (2006). E/I corrected paleolatitudes for the sedimen-
 768 tary rocks of the Baja British Columbia hypothesis. *Earth and Planetary Sci-
 769 ence Letters*, 242(1-2), 205–216. doi: 10.1016/j.epsl.2005.11.052

- 770 Linci, L., Tohver, E., Wilson, A., & Flint, S. (2013). Upper Permian magnetic
771 stratigraphy of the lower Beaufort Group, Karoo Basin. *Earth and Planetary
772 Science Letters*, 375, 123–134. doi: 10.1016/j.epsl.2013.05.017
- 773 Li, S., Li, Y., Tan, X., Wang, C., Han, Z., Xiao, S., ... Zhang, J. (2022). New paleo-
774 magnetic results of the Upper Cretaceous to Lower Eocene sedimentary rocks
775 from the Xigaze forearc basin and their tectonic implications. *Tectonophysics*,
776 837, 229433. doi: 10.1016/j.tecto.2022.229433
- 777 Li, Y., Kodama, K., & Smith, D. (2001). A compaction-corrected inclination for the
778 Middle Cretaceous Valle Group in Vizcaino Terrane, Baja California, Mexico:
779 preliminary results. In *Agu fall meeting abstracts* (pp. GP41A–0256).
- 780 Lovlie, R., & Torsvik, T. (1984). Magnetic remanence and fabric properties of
781 laboratory-deposited hematite-bearing red sandstone. *Geophys. Res. Lett.*,
782 11(3), 221–224. doi: 10.1029/GL011i003p00221
- 783 Lu, H. M., & Meng, X. K. (2010). Morin temperature and Néel temperature of
784 hematite nanocrystals. *The Journal of Physical Chemistry C*, 114(49), 21291–
785 21295. doi: 10.1021/jp108703b
- 786 McElhinny, M. W., & McFadden, P. L. (1997). Palaeosecular variation over the
787 past 5 Myr based on a new generalized database. *Geophysical Journal International*,
788 131(2), 240–252. doi: 10.1111/j.1365-246X.1997.tb01219.x
- 789 McFadden, P. L., & McElhinny, M. W. (1990). Classification of the reversal test in
790 palaeomagnetism. *Geophysical Journal International*, 103(3), 725–729. doi: 10
791 .1111/j.1365-246X.1990.tb05683.x
- 792 Meijers, M. J. M., Kaymakci, N., van Hinsbergen, D. J. J., Langereis, C. G.,
793 Stephenson, R. A., & Hippolyte, J.-C. (2010). Late Cretaceous to Pale-
794 ocene orocinal bending in the central Pontides (Turkey). *Tectonics*, 29(4).
795 doi: 10.1029/2009tc002620
- 796 Meng, J., Coe, R. S., Wang, C., Gilder, S. A., Zhao, X., Liu, H., ... Li, S. (2017).
797 Reduced convergence within the Tibetan Plateau by 26 Ma? *Geophysical Re-
798 search Letters*, 44(13), 6624–6632. doi: 10.1002/2017gl074219
- 799 Milanese, F., Rapalini, A., Slotznick, S. P., Tobin, T. S., Kirschvink, J., & Olivero,
800 E. (2019). Late Cretaceous paleogeography of the Antarctic Peninsula: New
801 paleomagnetic pole from the James Ross Basin. *Journal of South American
802 Earth Sciences*, 91, 131–143. doi: 10.1016/j.jsames.2019.01.012

- 803 Miller, J., James D., Green, J. C., Severson, M. J., Chandler, V. W., & Peterson,
804 D. M. (2001). *M-119 Geologic map of the Duluth Complex and related rocks,*
805 *northeastern Minnesota* (Tech. Rep.). Minnesota Geological Survey.
- 806 Mitchell, R., & Sheldon, N. (2009). Weathering and paleosol formation in the 1.1 Ga
807 Keweenawan Rift. *Precambrian Research*, 168(3-4), 271–283. doi: 10.1016/j/
808 .precamres.2008.09.013
- 809 Sun, W. W., & Kodama, K. P. (1992). Magnetic anisotropy, scanning electron mi-
810 croscopy, and X ray pole figure goniometry study of inclination shallowing in a
811 compacting clay-rich sediment. *Journal of Geophysical Research: Solid Earth*,
812 97(B13), 19599–19615. doi: 10.1029/92JB01589
- 813 Swanson-Hysell, N. L., Hoaglund, S. A., Crowley, J. L., Schmitz, M. D., Zhang,
814 Y., & Miller, J. D. (2021). Rapid emplacement of massive Duluth Com-
815 plex intrusions within the North American Midcontinent Rift. *Geology*. doi:
816 10.1130/G47873.1
- 817 Swanson-Hysell, N. L., Ramezani, J., Fairchild, L. M., & Rose, I. R. (2019). Failed
818 rifting and fast drifting: Midcontinent Rift development, Laurentia’s rapid mo-
819 tion and the driver of Grenvillian orogenesis. *GSA Bulletin*, 131(5-6), 913–940.
820 doi: 10.1130/B31944.1
- 821 Swanson-Hysell, N. L., Fairchild, L. M., & Slotznick, S. P. (2019). Primary
822 and secondary red bed magnetization constrained by fluvial intraclasts.
823 *Journal of Geophysical Research: Solid Earth*, 124(5), 4276–4289. doi:
824 10.1029/2018JB017067
- 825 Tan, X., Gilder, S., Kodama, K. P., Jiang, W., Han, Y., Zhang, H., ... Zhou, D.
826 (2010). New paleomagnetic results from the Lhasa block: Revised estima-
827 tion of latitudinal shortening across Tibet and implications for dating the
828 India–Asia collision. *Earth and Planetary Science Letters*, 293(3-4), 396–404.
829 doi: 10.1016/j.epsl.2010.03.013
- 830 Tan, X., & Kodama, K. P. (1998). Compaction-corrected inclinations from southern
831 California Cretaceous marine sedimentary rocks indicate no paleolatitudinal
832 offset for the Peninsular Ranges terrane. *Journal of Geophysical Research:*
833 *Solid Earth*, 103(B11), 27169–27192. doi: 10.1029/98jb02343
- 834 Tan, X., Kodama, K. P., Chen, H., Fang, D., Sun, D., & Li, Y. (2003). Paleomag-
835 netism and magnetic anisotropy of Cretaceous red beds from the Tarim basin,

- 836 northwest China: Evidence for a rock magnetic cause of anomalously shallow
 837 paleomagnetic inclinations from central Asia. *Journal of Geophysical Research: Solid Earth*, 108(B2). doi: 10.1029/2001jb001608
- 838
- 839 Tan, X., Kodama, K. P., & Fang, D. (2002). Laboratory depositional and
 840 compaction-caused inclination errors carried by haematite and their im-
 841 plications in identifying inclination error of natural remanence in red
 842 beds. *Geophysical Journal International*, 151(2), 475–486. doi: 10.1046/j.
 843 j.1365-246X.2002.01794.x
- 844 Tauxe, L. (2005). Inclination flattening and the geocentric axial dipole hypothe-
 845 sis. *Earth and Planetary Science Letters*, 233(3-4), 247–261. doi: 10.1016/j.
 846 .epsl.2005.01.027
- 847 Tauxe, L., & Kent, D. V. (1984). Properties of a detrital remanence carried by
 848 haematite from study of modern river deposits and laboratory redeposi-
 849 tion experiments. *Geophysical Journal International*, 76(3), 543–561. doi:
 850 10.1111/j.1365-246X.1984.tb01909.x
- 851 Tauxe, L., & Kent, D. V. (2004). A simplified statistical model for the geomag-
 852 netic field and the detection of shallow bias in paleomagnetic inclinations: was
 853 the ancient magnetic field dipolar? In *Geophysical Monograph Series* (pp.
 854 101–115). American Geophysical Union. doi: 10.1029/145GM08
- 855 Tauxe, L., Kent, D. V., & Opdyke, N. D. (1980). Magnetic components contributing
 856 to the NRM of Middle Siwalik red beds. *Earth and Planetary Science Letters*,
 857 47(2), 279–284. doi: 10.1016/0012-821X(80)90044-8
- 858 Tauxe, L., & Kodama, K. P. (2009). Paleosecular variation models for ancient times:
 859 Clues from Keweenawan lava flows. *Physics of the Earth and Planetary Interiors*,
 860 177(1), 31–45. doi: 10.1016/j.pepi.2009.07.006
- 861 Tauxe, L., Kodama, K. P., & Kent, D. V. (2008). Testing corrections for pa-
 862 leomagnetic inclination error in sedimentary rocks: A comparative ap-
 863 proach. *Physics of the Earth and Planetary Interiors*, 169(1), 152–165. doi:
 864 10.1016/j.pepi.2008.05.006
- 865 Tauxe, L., Shaar, R., Jonestrask, L., Swanson-Hysell, N. L., Minnett, R., Koppers,
 866 A. a. P., . . . Fairchild, L. (2016). PmagPy: Software package for paleomagnetic
 867 data analysis and a bridge to the MagNETics Information Consortium (MagIC)
 868 Database. *Geochemistry, Geophysics, Geosystems*, 17(6), 2450–2463. doi:

869 10.1002/2016GC006307

- 870 Tong, Y., Yang, Z., Mao, C., Pei, J., Pu, Z., & Xu, Y. (2017). Paleomagnetism of
871 Eocene red-beds in the eastern part of the Qiangtang Terrane and its impli-
872 cations for uplift and southward crustal extrusion in the southeastern edge of
873 the Tibetan Plateau. *Earth and Planetary Science Letters*, *475*, 1–14. doi:
874 10.1016/j.epsl.2017.07.026
- 875 Tong, Y.-B., Yang, Z., Zheng, L.-D., Xu, Y.-L., Wang, H., Gao, L., & Hu, X.-
876 Z. (2013). Internal crustal deformation in the northern part of Shan-Thai
877 Block: New evidence from paleomagnetic results of Cretaceous and Paleogene
878 redbeds. *Tectonophysics*, *608*, 1138–1158. doi: 10.1016/j.tecto.2013.06.031
- 879 Torsvik, T. H., Van der Voo, R., Preeden, U., Mac Niocaill, C., Steinberger, B.,
880 Doubrovine, P. V., ... Cocks, L. R. M. (2012). Phanerozoic polar wander,
881 palaeogeography and dynamics. *Earth-Science Reviews*, *114*(3), 325–368. doi:
882 10.1016/j.earscirev.2012.06.007
- 883 Vaes, B., Li, S., Langereis, C. G., & van Hinsbergen, D. J. J. (2021). Reliability
884 of palaeomagnetic poles from sedimentary rocks. *Geophysical Journal Interna-
885 tional*, *225*(2), 1281–1303. doi: 10.1093/gji/ggab016
- 886 van Andel, S. I., & Hospers, J. (1966). Systematic errors in the palaeomagnetic in-
887 clination of sedimentary rocks. *Nature*, *212*(5065), 891–893. doi: 10.1038/
888 212891a0
- 889 van Hinsbergen, D. J., Krijgsman, W., Langereis, C. G., Cornée, J.-J., Duermei-
890 jer, C. E., & van Vugt, N. (2007). Discrete Plio-Pleistocene phases of tilt-
891 ing and counterclockwise rotation in the southeastern Aegean arc (Rhodos,
892 Greece): early Pliocene formation of the south Aegean left-lateral strike-
893 slip system. *Journal of the Geological Society*, *164*(6), 1133–1144. doi:
894 10.1144/0016-76492006-061
- 895 van Hinsbergen, D. J. J., Dekkers, M. J., & Koc, A. (2010). Testing Miocene re-
896 magnetization of Bey Dağları: Timing and amount of Neogene rotations in SW
897 Turkey. *Turkish Journal of Earth Sciences*, *19*(2), 123–156.
- 898 van Hinsbergen, D. J. J., Lippert, P. C., Dupont-Nivet, G., McQuarrie, N.,
899 Doubrovine, P. V., Spakman, W., & Torsvik, T. H. (2012). Greater India
900 Basin hypothesis and a two-stage Cenozoic collision between India and Asia.
901 *Proceedings of the National Academy of Sciences*, *109*(20), 7659–7664. doi:

- 902 10.1073/pnas.1117262109
- 903 van Toorenenburg, K. A., Donselaar, M. E., & Weltje, G. J. (2018). The life cycle
904 of crevasse splays as a key mechanism in the aggradation of alluvial ridges and
905 river avulsion. *Earth Surface Processes and Landforms*, 43(11), 2409–2420.
906 doi: 10.1002/esp.4404
- 907 Vaughn, J., Kodama, K. P., & Smith, D. P. (2005). Correction of inclination shal-
908 lowing and its tectonic implications: The Cretaceous Perforada Formation,
909 Baja California. *Earth and Planetary Science Letters*, 232(1-2), 71–82. doi:
910 10.1016/j.epsl.2004.11.026
- 911 Westerweel, J., Roperch, P., Licht, A., Dupont-Nivet, G., Win, Z., Poblete, F., ...
912 Aung, D. W. (2019). Burma Terrane part of the Trans-Tethyan arc during
913 collision with India according to palaeomagnetic data. *Nature Geoscience*,
914 12(10), 863–868. doi: 10.1038/s41561-019-0443-2
- 915 Yan, M., Van der Voo, R., Tauxe, L., Fang, X., & M Parés, J. (2005). Shallow bias
916 in Neogene palaeomagnetic directions from the Guide Basin, NE Tibet, caused
917 by inclination error. *Geophysical Journal International*, 163(3), 944–948. doi:
918 10.1111/j.1365-246X.2005.02802.x
- 919 Zhang, Y., Huang, W., Huang, B., Hinsbergen, D. J. J., Yang, T., Dupont-Nivet,
920 G., & Guo, Z. (2018). 53–43 Ma deformation of eastern Tibet revealed by
921 three stages of tectonic rotation in the Gongjue Basin. *Journal of Geophysical
922 Research: Solid Earth*, 123(5), 3320–3338. doi: 10.1002/2018jb015443
- 923 Zhang, Y., Swanson-Hysell, N. L., Schmitz, M. D., Miller, J. D., & Avery, M. S.
924 (2021). Synchronous emplacement of the anorthosite xenolith-bearing Beaver
925 River diabase and one of the largest lava flows on Earth. *Geochemistry, Geo-
926 physics, Geosystems*, 22(10), e2021GC009909. doi: 10.1029/2021GC009909
- 927 Özdemir, , & Dunlop, D. J. (2014). Hysteresis and coercivity of hematite.
928 *Journal of Geophysical Research: Solid Earth*, 119(4), 2582–2594. doi:
929 10.1002/2013JB010739